



Evaluation of physical properties and bactericidal efficacy of chemically developed undoped and Mn (5, 10, 15wt%) doped ZnO nanoparticles

R. Sivasankari , M. Elango , J. Varuna & K. Thamizharasan

To cite this article: R. Sivasankari , M. Elango , J. Varuna & K. Thamizharasan (2020): Evaluation of physical properties and bactericidal efficacy of chemically developed undoped and Mn (5, 10, 15wt%) doped ZnO nanoparticles, Materials Technology, DOI: [10.1080/10667857.2020.1837542](https://doi.org/10.1080/10667857.2020.1837542)

To link to this article: <https://doi.org/10.1080/10667857.2020.1837542>



Published online: 27 Nov 2020.



Submit your article to this journal [↗](#)



Article views: 13



View related articles [↗](#)



View Crossmark data [↗](#)



Evaluation of physical properties and bactericidal efficacy of chemically developed undoped and Mn (5, 10, 15wt%) doped ZnO nanoparticles

R. Sivasankari^{a,b}, M. Elango^c, J. Varuna^c and K. Thamizharasan^a

^aResearch Scholar, R & D Center, Bharathiar University, Coimbatore, India; ^bDepartment of Physics, Sir Theagaraya College, Chennai, India; ^cDepartment of Physics, PSG College of Arts & Science, Coimbatore, India

ABSTRACT

Chemical precipitated and followed by calcinations is a versatile process for synthesising undoped ZnO and Mn (5, 10 and 15 wt%) doped ZnO nanoparticles at pH-10 and calcinations temperature of 450°C for 2 hours were followed for synthesising all the samples. The structural properties evaluated via XRD pattern revealed the hexagonal wurzite phase and with the grain size of 19 to 9 nm. Variation in the microstructural properties as function of dopant concentration was attributed using standard relations. The morphological and cross verification of structural properties were made via HRTEM analysis. Wide, direct allowed band gap property and narrow size distributed particles nature were confirmed through UV-visible absorption spectra with blue shifted peaks. The bandgap values got increased on increasing the dopant concentration. The presences of functional groups of the prepared samples were also confirmed by FTIR. Bands below 700 cm⁻¹ assigns the Metal-oxygen framework of the sample. The antibacterial efficiency of the prepared nanoparticles was evaluated for gram positive bacterial strains namely *Staphylococcus aureus* and *Bacillus subtilis*.

ARTICLE HISTORY

Received 17 July 2020
Accepted 11 October 2020

KEYWORDS

ZnO; Chemical precipitation; Physical properties; Bacterial properties

Introduction

Hexagonal wurzite phase ZnO nanoparticles are n-type semiconductor with wide band gap energy of 3.7 eV. The transition metal doping on ZnO nanoparticles further enhances the band gap in order to attain the comparatively size reduced particles. It is well admitted that ZnO nanoparticles exhibit numerous applications in every fields of science and technology like catalyst [1], gas sensors [2], cosmetic products [3], solar cells [4], antibacterial [5], antimicrobial [6] and anticancer agents [7]. Though zinc, a post-transition metal it finds a unique property to achieve these applications. ZnO nanoparticles can be prepared via sol-gel, co-precipitation, hydrothermal, sono-chemical, laser deposition and so on [8–12]. Ranjani viswanatha et al. [13] reported the absorption properties of size controlled Mn doped ZnO nanoparticles prepared via different synthesised conditions. Qianqian Gao et al. [14] discussed the stoichiometry of Mn doped ZnO nanosystems by correlating oxygen vacancies and Mn dopant concentration. Among the various synthesising routes, chemical co-precipitation method is facile, inexpensive and easy to access the steps. The chemical route for synthesising ZnO nanoparticles provides the suitable environment for the grain growth. The main objective of the paper is to prepare undoped and Mn (5, 10, 15 wt%) doped ZnO nanoparticles through chemical co-precipitation technique and the

evaluation of their physical properties such as structural, microstructural, morphological and optical properties.

Experimental procedure

Materials

Zinc acetate dihydrate (Zn(CH₃COO)₂·(H₂O)₂) (99.9% purity), sodium hydroxide (NaOH) and ethanol (CH₃CH₂OH) were used as the anionic, cationic precursor and solvent for preparation. Manganese acetate dihydrate (Mn(CH₃COO)₂·(H₂O)₂) (99.9% purity) was used as dopant precursor. All the precursor and solvent were purchased from MERCK and were used as received. The preparation of undoped and Mn (5, 10, 15 wt%) doped ZnO nanoparticles was carried out in the room temperature.

Synthesis

Undoped and transition metal Mn (5, 10, 15 wt%) doped ZnO nanoparticles were synthesised by chemical co-precipitation. Firstly, pure ZnO nanoparticles were prepared. Non-aqueous solutions of Zn(CH₃COO)₂·(H₂O)₂ and non-aqueous solutions of NaOH were separately prepared and were mixed in a round bottom flask. This solution mixture was stirred for about 1 hour at ambient temperature. Then the

milky precipitate was obtained at pH-10 and this pH is maintained under vigorous stirring. The precipitate was aged for about 8 hours. Finally the aged precipitate was washed thoroughly using organic solvents and centrifuged at 6000 rpm. The pellet was kept for calcination at 450°C for 2 hours. The undoped ZnO nanoparticles were prepared.

The Mn doped ZnO samples were prepared just by adding dissolved dopant precursor $\text{Mn}(\text{CH}_3\text{COO})_2 \cdot (\text{H}_2\text{O})_2$ at 5, 10, 15 wt% concentration while stirring of anionic solvent, followed by the addition of cationic precursor to the above mixture. The colour of solution mixture gets changed from colourless to turbid dirty white in colour and the formation of precipitate was occurred. The residue was maintained at pH-10. The precipitate was allowed to stir for 8 hours which is an ageing period for completion of reaction. The aged samples were washed thoroughly for several times using organic solvents. The well cleaned samples were centrifuged at 6000 rpm and the supernatant was removed and the pellet was dried at 450°C for 2 hours. All the above procedures were followed for the preparation other samples namely 10 wt% and 15 wt% Mn doped ZnO sample. This paper discuss about undoped and (5, 10, 15 wt%) Mn doped ZnO samples.

Characterisation

The prepared samples were characterised through various analytical techniques. Structural analysis was done using X-ray diffraction (XRD) and high resolution transmission electron microscopy (HRTEM). The composition analysis was done energy dispersive analysis (EDS). Optical studies were performed using UV-visible absorption (UV-Vis) and Fourier transform infrared (FT-IR) spectroscopy. The crystalline nature and phase purity of the prepared samples was identified by X-Ray diffraction technique using Shimadzu diffractometer which uses Cu-K α line (1.5406 Å) from 10° to 90°. The d-spacing and crystallinity of the samples were confirmed through HRTEM (JEOL JEM 3010) of 200 kV accelerating voltage with lattice resolution of 0.17 nm and 0.10 nm. The compositional analysis was also done along with HRTEM using BRUKER QUANTAX EDS X-Flash detector. The band gap and particle size analysis was done using Varian Cary 5E Spectrometer in the range of 200–1200 nm whose slit width is of 0.01 nm of optimum control over data resolution. The functional groups of the prepared samples were identified through FTIR spectra taken through BRUKER IFS 66 W with rapid scan at 12 cm⁻¹ spectral resolution and at the scanning rate of 25 cycles per minute. The

FTIR spectra scans over 4000–400 cm⁻¹ range using KBr pellets at room temperature.

Bactericidal analysis

The antibacterial activity of pure and various concentration of Mn doped ZnO was performed against Gram-positive (*Bacillus subtilis* and *Staphylococcus aureus*) bacterial strains by disc diffusion method. The microorganisms were inoculated in the fresh nutrient broth and incubated to get required turbidity. The nutrient agar plate was swabbed with the test bacterial culture and various concentrations of sample discs (μg) (discs are soaked overnight in nanoparticle suspension) was added into the well. After 24 h incubation at 37°C, the antibacterial activity was measure based on the diameter of the zone of clearance.

Results and discussion

X-ray diffraction studies

The structural properties of the undoped and transition metal Mn (5, 10, 15 wt%) doped ZnO nanoparticles investigated through XRD analysis at room temperature. Figure 1. showed the X-ray diffraction profile for undoped and Mn (5, 10 and 15 wt%) doped ZnO system. Hexagonal wurtzite structure (Space group: p63mc) was confirmed by observing the miller planes (100), (002), (101), (102), (110), (103) at 31.8°, 34.3°, 36.8°, 47.5°, 56.4° and 62.9° respectively which accord well with the JCPDS Card no. 89-0511 [15]. No impurities or secondary phase peaks were observed in the XRD pattern, which indicates the phase purity of the prepared samples.

A slight shift in the peak position towards lower diffraction angle (2θ) value was observed which is due to the insertion of Mn²⁺ dopants as substitutional defects in ZnO lattices on obeying Vegard's law. Since the dopants are incorporated in the ZnO nanosystem, lattice distortion might be due to two possible reasons.

(1). Mn²⁺ ions occupy the interstitial position and cause the lattice to expand.

(2). Mn²⁺ ions replace the Zn²⁺ ions and occupy its lattice position (substitution) which causes a reduction in the lattice. Vijayakumar et al found the same result while encapsulating the Mn-doped Zinc nanoparticles with PEG [16]. Jong et al. states that after Mn doping, the lattice parameter of ZnO nanoparticles commence to increase that might be due to the ionic radii of Mn²⁺ (0.66 Å) is greater than Zn²⁺ (0.60 Å) which ultimately shows that Mn may occupy an interstitial position as dopant [17]. In the present study, we observed mill variation in the lattice constants value concerning

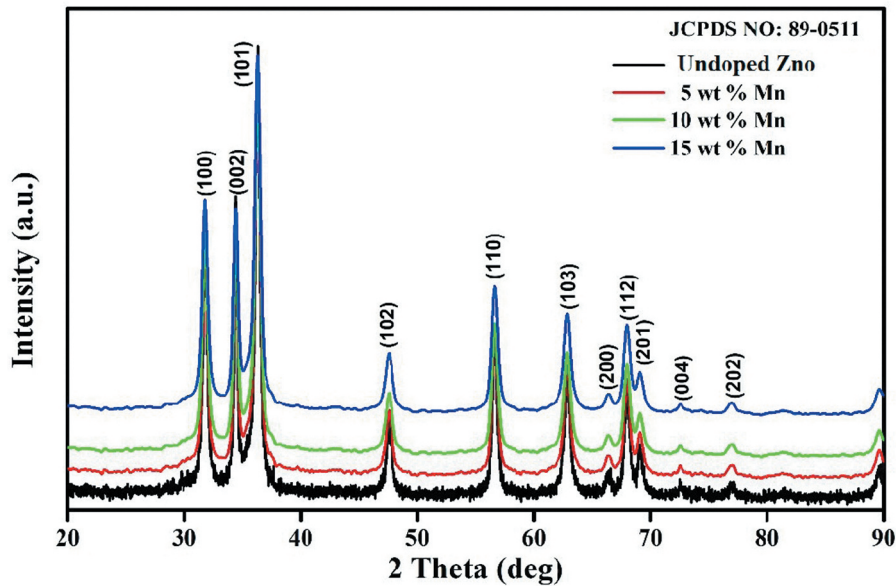


Figure 1. X-ray diffractogram of undoped and (5, 10, 15 wt%) Mn doped ZnO.

previous reports which further validate the substitutional insertion of Mn ions in the host matrices. Figure 2 depicts the lattice parameter against dopant concentration. As the Mn dopant concentration increases, the c/a ratio also increases, but the number of unit cells per volume gets reduced which indicates the structural changes and reduction in the crystalline nature of the samples.

The crystallite size was calculated using the Debye Scherrer equation,

$$D = K\lambda/\beta\cos\theta \quad (1)$$

Where K is a constant, λ is the wavelength of the radiation (1.5406\AA) and β is full width half maximum of a plane. From Table 1, Crystallite size reduces from 19.3 nm to 9.32 nm upon increasing the dopant concentration which eventually due to increased microstrain in the ZnO nanosystem. The crystallite size was also reduced on doping which may due to the introduction of impurity ions that hinders the grain growth of ZnO nanoparticles.

Lattice parameters (a , c), unit cell volume, crystallite volume, dislocation density, microstrain values were also evaluated from the standard relations [18],

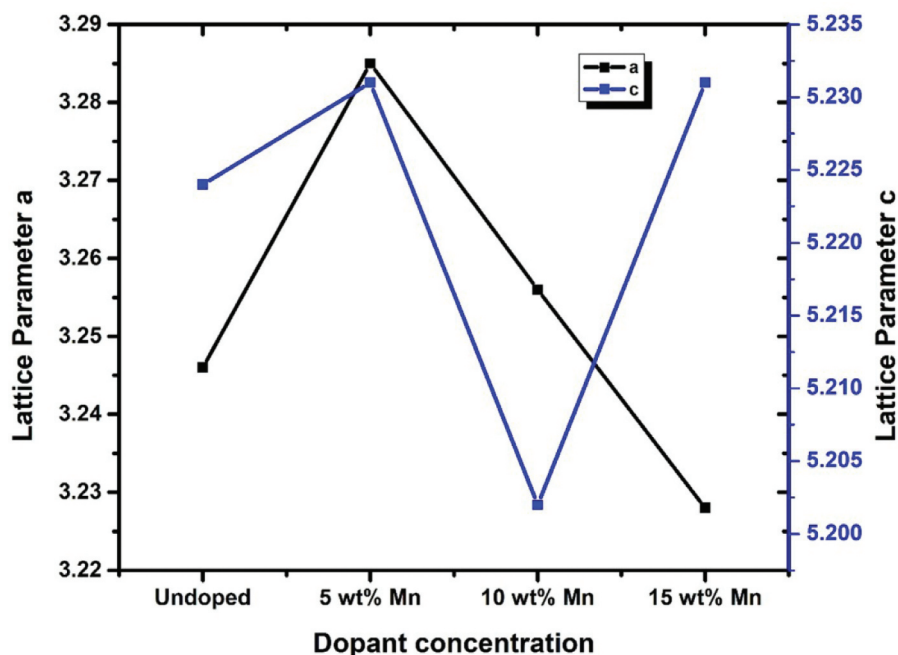


Figure 2. Dopant concentration vs lattice parameter.

Table 1. Microstructural properties of undoped and (5, 10, 15 wt%) Mn doped ZnO.

| Sample | 2 θ | Crystallite Size | Lattice parameter | | | Crystallite volume | Dislocation density | Microstrain | $N_D = \frac{V}{\rho}$ ($\times 10^6$) |
|-----------|------------|------------------|-------------------|-------|---------------|--------------------|---------------------|-------------|---|
| | | | a | c | $\frac{c}{a}$ | | | | |
| Undoped | 31.8 | 19.3 | 3.246 | 5.224 | 1.6085 | 7.189 | 2.68 | 1.789 | 0.150 |
| 5 wt% Mn | 31.72 | 15.32 | 3.285 | 5.231 | 1.5925 | 3.595 | 4.271 | 2.26 | 0.313 |
| 10 wt% Mn | 31.75 | 12.10 | 3.256 | 5.202 | 1.5978 | 1.771 | 6.830 | 2.86 | 0.253 |
| 15 wt% Mn | 31.99 | 9.32 | 3.228 | 5.231 | 1.6207 | 0.8095 | 0.011 | 3.717 | 0.197 |

The microstructural properties found from the XRD diffractogram are tabulated (Table 1). The dopant induced microstrain inside the system hinders the grain growth and thus, we observe the grain growth reduction upon doping. Microstructural properties like dislocation density, crystallite volume and several crystallites are also found to be correlated with each other.

UV-Visible Spectroscopy

The optical properties of the prepared samples were studied through UV-Vis spectra. Figure 3 reveals the optical property of Mn-doped ZnO nanoparticles which can be defined by the absorbance of the prepared samples. The wavelength observed and obtained bandgap by the samples were tabulated in Table 2. For semiconductor nanosystems, the absorption cross section is correspondingly higher because of their high geometrical surface area. This factor gives rise to every photon cross the nanosystems within the part of the absorption cross-section gets absorbed by the nanoparticles. Hence, the prepared extrinsic ZnO semiconductor nanoparticles showcased their band edge absorption at around 396 nm. In addition increase of absorption intensity with all composition of Mn was recorded. This reveals that the spin exchange interaction between the d orbitals of Mn^{2+} and band electrons of ZnO crystal lattice. When alkali metal oxides doped

with ZnO more number of electrons can jump from ground state to excited state. But Cai et al. give out the more dopant concentration of Mn doping can decrease the intensity due to the large number of defect sites produced in the ZnO lattice [19].

The optical band gap of the prepared from the relation,

$$E_g = \frac{1240}{\lambda} (eV) \quad (2)$$

Where λ is the wavelength of the absorption spectrum (nm) [20]

The optical properties of the prepared samples were studied through UV-Vis spectra. Figure 3 reveals the optical property of Mn (5, 10 and 15 wt%) doped ZnO nanoparticles that can be defined by the absorbance of the prepared samples. The wavelength observed and obtained band gap by the samples were tabulated in Table 2. For semiconductor nanosystems, the absorption cross-section is correspondingly higher because of their high geometrical surface area. This factor gives rise to every photon cross the nanosystems within the part of the absorption cross-section gets absorbed by the nanoparticles. Hence, the prepared extrinsic ZnO semiconductor nanoparticles showcased their band edge absorption at around 396 nm. The particle size of the prepared samples were found from Meulenkemp formula,

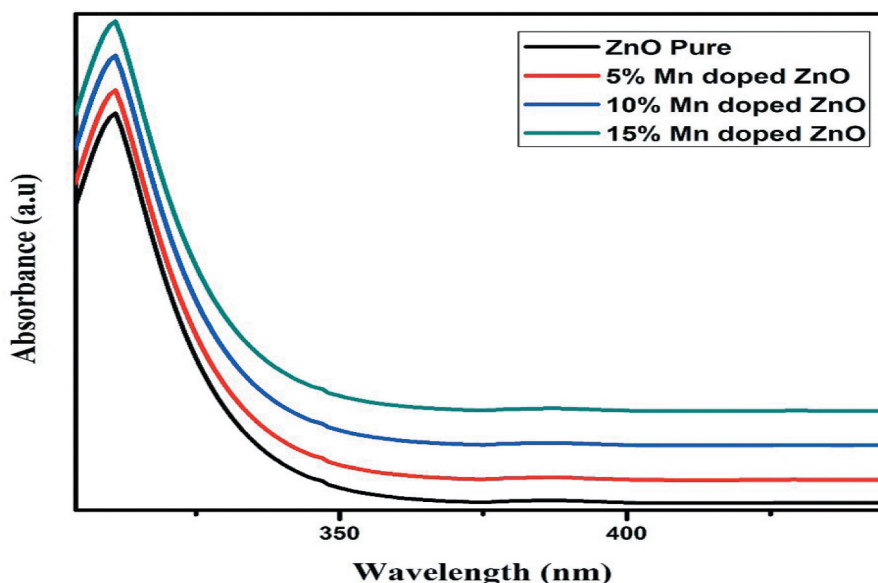
**Figure 3.** UV-visible spectra of undoped and (5, 10, 15 wt%) Mn doped ZnO.

Table 2. Optical properties of undoped and (5, 10, 15 wt%) Mn doped ZnO.

| Sample | Wavelength (nm) | Band gap (eV) | Particle size (Meulenkemp) (nm) | Particle size (effective mass approximation) (nm) |
|-----------|-----------------|---------------|---------------------------------|---|
| Undoped | 274.5 | 4.517 | 7.2564 | 20.45 |
| 5 wt% Mn | 270 | 4.592 | 7.1617 | 19.195 |
| 10 wt% Mn | 267 | 4.6441 | 7.0990 | 18.411 |
| 15 wt% Mn | 265 | 4.6792 | 7.0572 | 17.91 |

$$1240/\lambda^{1/2} = [a + (b/D^2)] - (c/D) \quad (3)$$

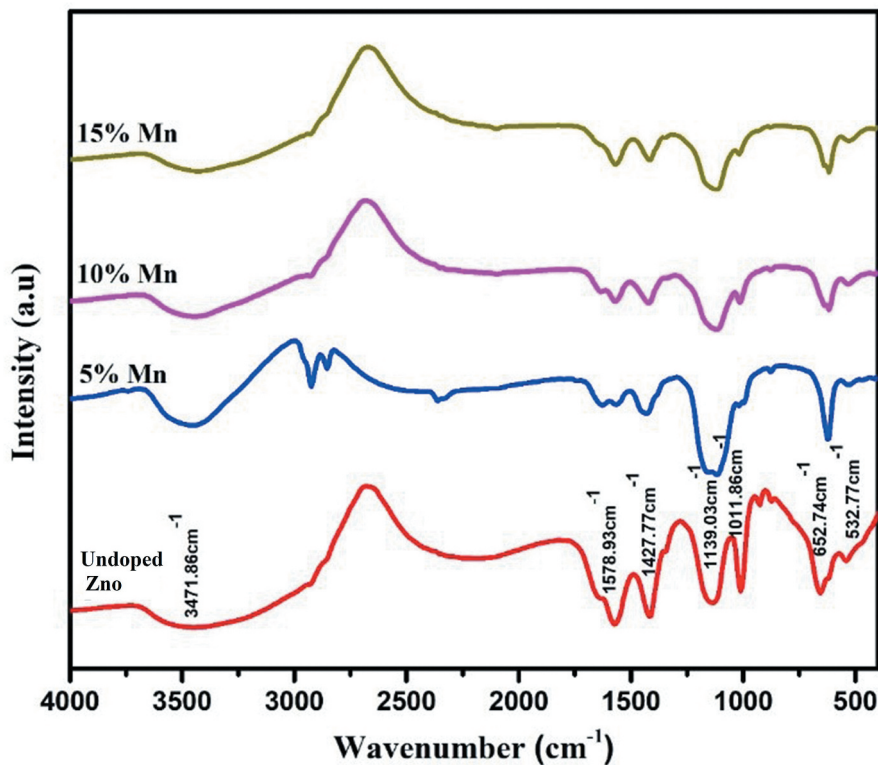
Where, $a = 3.301$, $b = 294$ and $c = 1.09$ respectively. The obtained particle sizes were 7.256, 7.161, 7.099 and 7.057 nm for undoped, 5 wt% Mn, 10 wt% Mn and 15 wt% Mn doped ZnO respectively. By increasing the dopant concentration, the particle size was reduced that might be due to the hindrance of Ostwald's ripening process and also the growth of the particles obeys the electronic double layer theory, in which, the net negative charge around the individual particles gets decreased due to the inclusion of anionic dopant. From EDS analysis, a very limited number of Mn ions are substituted in the place of Zn. Hence the maintaining the negative layer around the particle protects the particle from agglomeration and grain growth of the same. The particle sizes can also be found from effective mass approximation,

$$R^2 = h^2/8(\Delta E)[1/m_e^* + 1/m_h^*] \quad (4)$$

The particle size of the prepared samples were 20.45, 19.19, 18.411 and 17.917 nm for undoped, 5 wt% Mn, 10 wt% Mn, 15 wt% Mn respectively.

FTIR Spectroscopy

FTIR is a sensitive and effective way to determine the functional groups of the prepared samples with high spectral resolution over a wide spectral data. Figure 4 represents the FT-IR spectra which expose the stretching and bending vibrating modes of the synthesised undoped and Mn (5, 10 and 15 wt%) doped ZnO samples. Similar type of transmission spectra was obtained by Neha Sharma et.al., for Manganese and iron doped Zinc nanoparticles. The transmission spectra below 700 cm^{-1} indicates that the grown particles are in nano size [21]. The broad absorption band at 3457.72 cm^{-1} , 3471.86 cm^{-1} , 3502.40 cm^{-1} and 1561.34 cm^{-1} , 1568.54 cm^{-1} , 1578.93 cm^{-1} attributes the stretching mode of superfluous -OH groups and H-O-H bending mode of water molecules [22]. The band at 525.57 cm^{-1} assigns the characteristic peak for ZnO sample. Upon doping characteristic peaks slightly shift towards higher wavenumber region to 535.77 cm^{-1} . FTIR explores the Zn-O/Mn-O/Ni-O bands below 1000 cm^{-1} which attributes the metal-oxygen bonding [23].

**Figure 4.** FTIR spectra of undoped and (5, 10, 15 wt%) Mn doped ZnO.

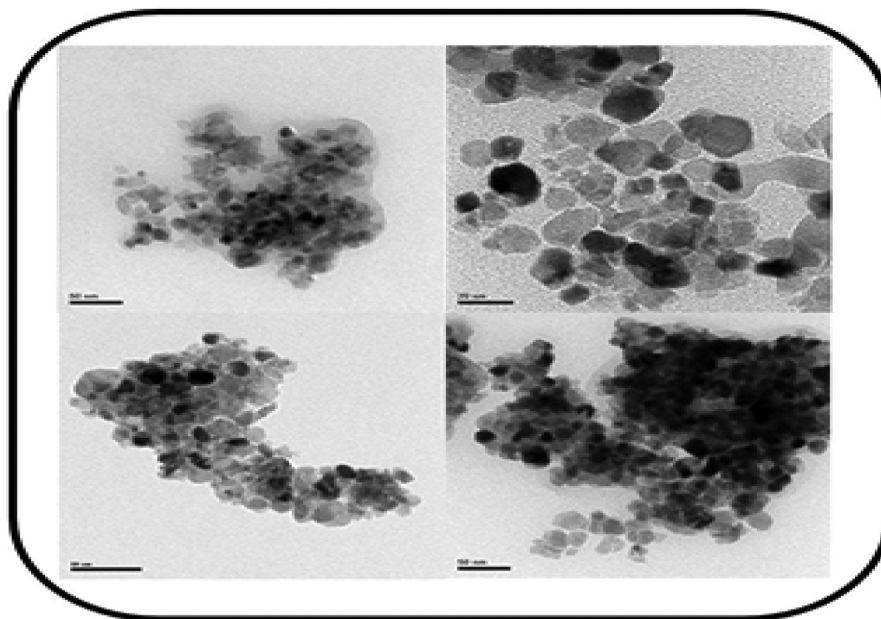


Figure 5. HRTEM Images of undoped and 5, 10, 15 wt% Mn doped ZnO.

HRTEM

The micrographs in [Figure 5](#) portrait the spherical morphology and wide particle distribution of the prepared samples. We can also witness that there is no morphological variation upon increasing the dopant concentration on Mn (5, 10 and 15 wt%) doped ZnO nanosystem [24]. But it reveals that the particles are widely distributed with weak agglomeration for prepared samples. This agglomeration gets reduced on introducing dopants which might be due to the low surface energy caused by the dopants. But at higher doping there might be seen cluster of particles with reduced particle size. This plausible change of distribution can also found in Ca doped nanostructures [25]. The SAED pattern elucidates the further confirmation of hexagonal wurzite structure of Mn incorporated ZnO nanosystem whose results are matched well with the XRD data. The EDS spectra [Figure 6](#) clearly explicits the elemental composition of the samples.

BACTRICEDAL ANALYSIS

[Figures 7](#) and [8](#) show the antibacterial activity of pure ZnO and various concentration of Mn doped (5, 10, and 15 wt %) ZnO nanoparticles against Gram-positive (*S. aureus*) and *B. subtilis* bacterias'. Pure ZnO nanoparticles reveal less significant antibacterial activity, whereas the Mn doped ZnO nanoparticles exhibited potent antibacterial activity against Gram-positive bacteria. The greater number of Reactive Oxygen Species (ROS) is mainly attributed to the small crystallite size of the Mn (5, 10 and 15 wt%) doped ZnO NPs, which is agreed well with the XRD results, an increase in oxygen vacancies and the diffusion ability of the reactant molecules. In the present investigation, the antibacterial effect of the Mn doped ZnO NPs samples is mainly due to the combination of various factors such as ROS and the release of Zn^{2+} along with Mn^{2+} ions [26].

Enhanced bioactivity is also presumed to the generation of hydrogen peroxide (H_2O_2) from the Mn doped ZnO nanoparticles top layers which is

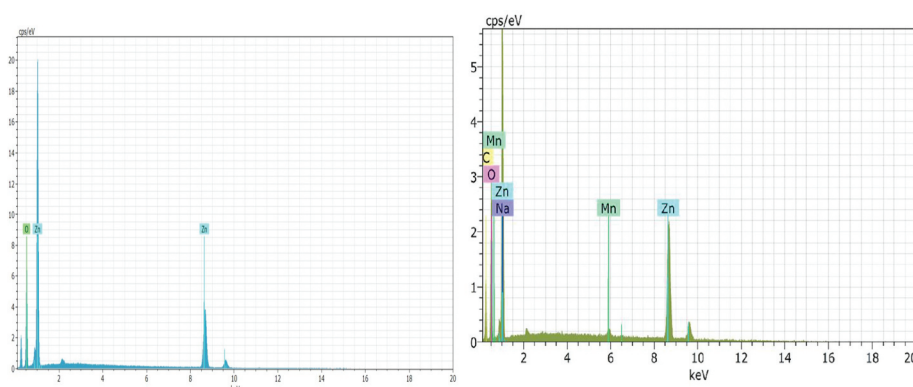


Figure 6. EDS analysis of undoped and Mn doped ZnO.

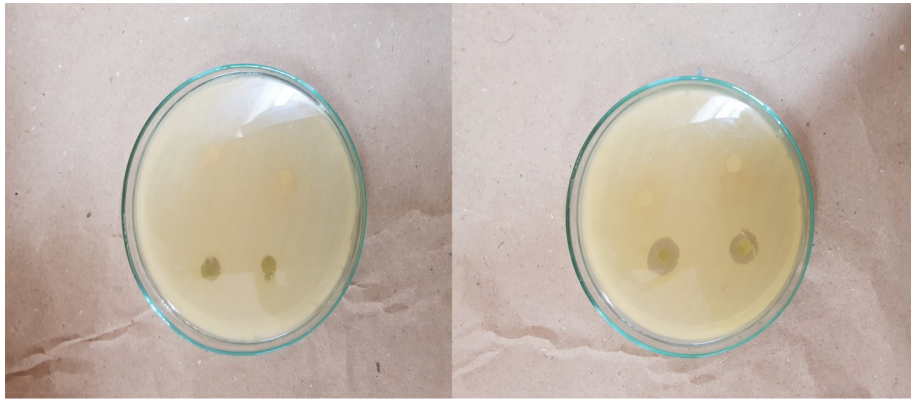


Figure 7. Bactericidal efficacy of ZnO nanoparticles against *S. aureus* and *B. subtilis*.



Figure 8. Bactericidal study of Mn doped ZnO nanoparticles against *S. aureus* and *B. subtilis*.

associated with the Zn^{2+} and/or Mn^{2+} ions. The above layers favour the generation of highly reactive species such as OH^- , H_2O_2 and O_2^{2-} . They then react with hydrogen ions to produce molecules of H_2O_2 . The generated H_2O_2 can penetrate into the cell membrane and kills the bacteria. The obvious nature of high surface to volume ratio of the nanoparticulate system paves path to enhance the generation of highly ROS systems against the given gram positive bacteria [27]. While comparing bacteria, it has been observed that Mn doped ZnO nanoparticles show strong antibacterial activity towards *S. aureus* than *B. subtilis*. It is understood that the gram-positive bacteria has the different structure and thickness of peptide glycans in the cell wall which prevents them from the killing agents. Our results show that the doping of Mn into the ZnO matrices enhances the killing efficiency of the pristine ZnO and shows the large area of zone of incubation.

Conclusion

Nanosized ZnO and Mn (5, 10 and 15 wt%) doped ZnO particles with an average sized of 20 nm have chemically developed and doping, their size reduced around 10 nm. The effect of doping on the basic

properties of prepared materials has evaluated by standard analytical methods. The properties such as crystalline, phase purity, morphology, optical absorption and chemical inertness have studied. Mn doping reduces the crystallite size. The zero influence of Mn doping has revealed from the structural investigation. Blue shifted band edge absorption at around 396 nm for all samples ensures the insertion of doping ion into host lattice and obeys the quantum confinement effect that yields degeneracy of energy levels due to the reduced size of the particles. The presence of the functional groups on the surface of the nanoparticles confirmed through the FT-IR spectroscopic study. The HRTEM results confirmed the monodispersed spherical morphology with less agglomerated state of the particles. The prepared Mn-doped ZnO nanoparticles are used as the antibacterial materials for gram-positive bacteria strains *S. aureus* and *B. subtilis*. Finally, revealed that ZnO nanoparticles prepared through an inexpensive and reliable method has been used for photovoltaic applications and medical applications.

Disclosure statement

No potential conflict of interest was reported by the authors.

References

- [1] Strunk J, Kähler K, Xia X, et al. Surface Science The surface chemistry of ZnO nanoparticles applied as heterogeneous catalysts in methanol synthesis. *Surf Sci.* 2009;603(10–12):1776–1783.
- [2] Wang, J. X., Sun, X. W., Yang, Y., Huang, H., Lee, Y. C., Tan, O. K., & Vayssieres, L. (2006). Hydrothermally grown oriented ZnO nanorod arrays for gas sensing applications. *Nanotechnology*, 17(19), 4995.
- [3] Paper O. Safety assessment by multiphoton fluorescence/second harmonic generation/hyper-rayleigh scattering tomography of zno nanoparticles. *Skin Pharmacol Physiol.* 2012;219–226. DOI:10.1159/000338976.
- [4] Beek BWJE, Wienk MM, Janssen RAJ. Hybrid Solar Cells from Regioregular Polythiophene and ZnO Nanoparticles. *Adv Funct Mater.* 2006;1112–1116. DOI:10.1002/adfm.200500573.
- [5] Xie Y, He Y, Irwin PL, et al. Antibacterial activity and mechanism of action of zinc oxide nanoparticles against campylobacter jejuni. *Appl Environ Microbiol.* 2011;77(7):2325–2331. .
- [6] Yu J, Zhang W, Ghasaban S, et al. Enhanced bioactivity of ZnO nanoparticles — an antimicrobial study. *Sci Technol Adv Mater.* 2008. DOI:10.1088/1468-6996/9/3/035004
- [7] Xia T, Kovochich M, Liang M, et al. Comparison of the mechanism of toxicity of zinc oxide and cerium oxide nanoparticles based on dissolution and oxidative stress properties. *ACS nano.* 2008;2(10):2121–2134.
- [8] Vafaee M, Ghamsari MS. Preparation and characterization of ZnO nanoparticles by a novel sol – gel route. *Mater Lett.* 2007;61:3265–3268. .
- [9] Hameed, A. S. H., Karthikeyan, C., Sasikumar, S., Kumar, V. S., Kumaresan, S., & Ravi, G. (2013). Impact of alkaline metal ions Mg 2+, Ca 2+, Sr 2+ and Ba 2+ on the structural, optical, thermal and antibacterial properties of ZnO nanoparticles prepared by the co-precipitation method. *Journal of Materials Chemistry B*, 1(43), 5950-5962.doi:10.1039/C3TB21068E.
- [10] Maryanti E, Damayanti D, Gustian I, et al. Synthesis of ZnO nanoparticles by hydrothermal method in aqueous rinds extracts of Sapindus rarak DC. *Mater Lett.* 2014;118:96–98.
- [11] Khan, S. H., Pathak, B., & Fulekar, M. H. (2016, April). Development of zinc oxide nanoparticle by sonochemical method and study of their physical and optical properties. In *AIP Conference Proceedings* (Vol. 1724, No. 1, p. 020108). AIP Publishing LLC.doi.org/10.1063/1.4945228.
- [12] Kawakami, M., Hartanto, A. B., Nakata, Y., & Okada, T. (2003). Synthesis of ZnO nanorods by nanoparticle assisted pulsed-laser deposition. *Japanese Journal of Applied Physics*, 42(1A), L33.doi:10.1143/JJAP.42.L33.
- [13] Viswanatha R, Sapra S, Sen Gupta S, et al. Synthesis and characterization of Mn-doped ZnO nanocrystals. *J Phys Chem A.* 2004;108(20):6303–6310. .
- [14] Gao Q, Dai Y, Yu Q, et al. Defect-induced structural and ferromagnetic properties of hydrogenated Mn-doped ZnO film. *J Mater Sci.* 2016 Jan 1;27(1):697–704.
- [15] Zak AK, Majid WHA, Abrishami ME, et al. X-ray analysis of ZnO nanoparticles by Williamson e Hall and size e strain plot methods. *Solid State Sci.* 2011;13. DOI:10.1016/j.solidstatesciences.2010.11.024.
- [16] Vijayakumar G, Boopathi G, Elango M. In vitro cytotoxic efficacy of PEG encapsulated manganese-doped zinc oxide nanoparticles on hepatocellular carcinoma cells. *Mater Technol.* 2019;34(13):807–817.
- [17] Cong CJ, Liao L, Li JC, et al. Synthesis, structure and ferromagnetic properties of Mn-doped ZnO nanoparticles. *Nanotechnology.* 2005;981. DOI:10.1088/0957-4484/16/6/060.
- [18] Magesh G, Bhoopathi G, Nithya N, et al. Superlattices and microstructures tuning effect of polysaccharide chitosan on structural, morphological, optical and photoluminescence properties of ZnO nanoparticles. *Superlattices Microstruct.* 2018;117:36–45.
- [19] Cai XY, Liu YJ, Zeng H, et al. Synthesis and characterisation of alkali metal (Mn, Fe) oxide–ZnO nanorod composites and their photocatalytic decolourization of rhodamine B under visible light. *Mater Technol.* 2012;27(5):380–387. .
- [20] Ashokkumar M, Muthukumar S. Microstructure, optical and FTIR studies of Ni, Cu co-doped ZnO nanoparticles by co-precipitation method. *Opt Mater (Amst).* 2014;37:671–678.
- [21] Sharma N, Jandaik S, Kumar S, et al. Synthesis, characterisation and antimicrobial activity of manganese- and iron-doped zinc oxide nanoparticles. *J Exp Nanosci.* 2016;11(1):54–71. .
- [22] Muthukumar S, Gopalakrishnan R. Structural, FTIR and photoluminescence studies of Cu doped ZnO nanopowders by co-precipitation method. *Opt Mater (Amst).* 2012;34(11):1946–1953.
- [23] Ā JZ, Zhao F, Wang Y, et al. Size-controlled synthesis of ZnO nanoparticles and their photoluminescence properties.. *J Lumin.* 2007;122–123:195–197.
- [24] Hammad TM, Griesing S, Wotocek M, et al. Optical and magnetic properties of Zn 0.98 Mn 0.02 O nanoparticles. *Appl Nanosci.* 2013;3(2):153–159. .
- [25] Misra KP, Kumawat A, Shahee A, et al. Effect on optical and structural parameters in heavy Ca-doped ZnO nanostructures. *Mater Technol* 2020;1–12. DOI:10.1080/10667857.2020.1776028.
- [26] Premanathan M, Karthikeyan K, Jeyasubramanian K, et al. Selective toxicity of ZnO nanoparticles toward Gram-positive bacteria and cancer cells by apoptosis through lipid peroxidation. *Nanomed Nanotechnol Biol Med.* 2011;7(2):184–192.
- [27] Xie Y, Yiping H, Irwin PL, et al. Antibacterial Activity and Mechanism of Action of Zinc Oxide Nanoparticles against *Campylobacter jejuni*. *Appl Environ Microbiol.* 2011;77(7):2325–2331.